materials

MDPI

Article

$Al_{13}Fe_4$-Al Composites with Nanocrystalline Matrix Manufactured by Hot-Pressing of Milled Powders

Marek Krasnowski [1,*], Stanislaw Gierlotka [2] and Dariusz Zasada [3]

[1] Faculty of Materials Science and Engineering, Warsaw University of Technology, Woloska 141, 02-507 Warsaw, Poland
[2] Institute of High Pressure Physics, Polish Academy of Sciences, Sokolowska 29/37, 01-142 Warsaw, Poland; xray@unipress.waw.pl
[3] Faculty of Advanced Technologies and Chemistry, Military University of Technology, Kaliskiego 2, 00-908 Warsaw, Poland; dariusz.zasada@wat.edu.pl
* Correspondence: marek.krasnowski@pw.edu.pl; Tel.: +48-22-234-87-16

Abstract: The paper describes composites with the matrix containing a nanocrystalline intermetallic $Al_{13}Fe_4$ phase and microcrystalline aluminium. Mechanically alloyed $Al_{80}Fe_{20}$ powder, containing a metastable nanocrystalline Al_5Fe_2 phase, was mixed with 20, 30, and 40 vol.% of Al powder and consolidated at 750 °C under the pressure of 7.7 GPa. During the consolidation, the metastable Al_5Fe_2 phase transformed into a nanocrystalline $Al_{13}Fe_4$ phase. In the bulk samples, $Al_{13}Fe_4$ areas were wrapped around by networking Al regions. The hardness of the $Al_{13}Fe_4$-Al composites was in the range of 4.52–5.50 GPa. The compressive strength of the $Al_{13}Fe_4$-30%Al and $Al_{13}Fe_4$-40%Al composites was 805 and 812 MPa, respectively, and it was considerably higher than that of the $Al_{13}Fe_4$-20%Al composite (538 MPa), which failed in the elastic region. The $Al_{13}Fe_4$-30%Al and $Al_{13}Fe_4$-40%Al composites, in contrast, showed some plasticity: namely, 1.5% and 9.1%, respectively. The density of the produced composites is in the range of 3.27–3.48 g/cm^3 and decreases with the increase in the Al content.

Keywords: metallic composites; intermetallics; nanocrystalline materials; mechanical alloying; powder compaction

Citation: Krasnowski, M.; Gierlotka, S.; Zasada, D. $Al_{13}Fe_4$-Al Composites with Nanocrystalline Matrix Manufactured by Hot-Pressing of Milled Powders. *Materials* **2022**, *15*, 4241. https://doi.org/10.3390/ma15124241

Academic Editor: Joan-Josep Suñol

Received: 30 December 2021
Accepted: 30 May 2022
Published: 15 June 2022

1. Introduction

Aluminium-based alloys are characterised by low density and good corrosion resistance. Among aluminium alloys, attention is attracted by, i.a., intermetallic phases of the Fe-Al system [1]. They have advantageous properties: a high specific strength and stiffness, good strength at intermediate temperatures, and excellent corrosion resistance at elevated temperatures [1]. Properties such as hardness and strength can be improved when iron aluminides have a nanocrystalline structure [2,3]. A well-known method of producing nanocrystalline materials is mechanical alloying (MA), followed by the consolidation of milled powders [4]. However, most consolidation techniques do not allow for obtaining of truly nanocrystalline samples that are large in size and free from artefactual defects formed during consolidation [5]. It was observed that such defects are a frequent cause of a lack of plasticity in consolidated samples [6]. These defects are often micropores between weakly bound powder particles, and they cause bulk nanocrystalline materials to crack at stresses lower than the yield strength. Therefore, the technological processes of bulk nanocrystalline materials can be treated as critical factors influencing their low ductility, and the key to its improvement is the consolidation of the material free of artefact-like defects [6].

High-temperature consolidation of mechanically alloyed powders, with a nanocrystalline structure preserved, is a task that is difficult to perform. The application of high temperatures, which is required to achieve good quality consolidation, can lead to excessive

grain growth. As we previously demonstrated, application of high pressure during consolidation inhibits grain growth and maintains the nanocrystalline structure of the pressed powder [7,8].

It was reported that the presence of larger grains in a nanocrystalline matrix (bimodal grain distribution) can improve a material's ductility in comparison with samples containing only nanometric grains [9]. A grain size distribution containing a fraction of grains large enough to maintain dislocation activity enables strain hardening, and thus favours an increase in ductility [6]. This prompted us to modify the microstructure of the consolidated powders to improve the ductility of the bulk materials [10,11]. We, therefore, produced the composite materials comprising a nanocrystalline intermetallic as a matrix and aluminium as a binder [10,11]. Ductile aluminium was to be distributed in the form of a "network" between hard nanocrystalline particles. The expected effect of the presence of a soft aluminium "network" was to improve the quality of bonding nanocrystalline particles into bulk material and, being a ductile component of the composite, to improve the plasticity of material. Micrometric aluminium grains contribute to the plastic deformation, and they may release stress concentrations and, hence, retard crack initiation and propagation [12]. The introduction of aluminium lowered the final density of the composites but also resulted in a decrease in the material hardness. Powders with nanocrystalline structure intended to form the matrix were produced by mechanical alloying [10,11]. They were then mixed with Al powder and subjected to short-term low-energy milling, which ensured even distribution of Al in the powder material. Mixtures prepared in such a way were consolidated into bulk form [10,11].

There are very few publications describing bulk materials containing ultrafine and larger grains, obtained by mixing nanocrystalline and microcrystalline powders, as well as the subsequent consolidation [9,12]. Apart from those reported by our group [10,11,13], no works related to nanocrystalline powders mixed with microcrystalline aluminium were found. It is, therefore, worth noting that the nanocrystalline phase-Al composites, as well as their technology, are innovative.

Recently, we prepared Al_3Ni_2-Al [10] and Al_5Fe_2-Al [11] composites with a nanocrystalline intermetallic matrix and various content of microcrystalline Al. The increase in composites' plasticity with the increase in Al content was observed in both cases. In the present work, composites with the matrix containing a nanocrystalline intermetallic $Al_{13}Fe_4$ phase and microcrystalline Al are being reported. The $Al_{13}Fe_4$ intermetallic phase has the density lower than the Al_3Ni_2 or Al_5Fe_2 intermetallic phases, and hence, the composites produced in this work will have a lower density than those reported previously. Based on the results of the previous studies [14], the alloy with $Al_{80}Fe_{20}$ stoichiometry was selected for the production of $Al_{13}Fe_4$ phase.

2. Materials and Methods

$Al_{80}Fe_{20}$ (at.%) elemental powders mixture was mechanically alloyed under argon atmosphere in a SPEX 8000 D shaker ball mill (SPEX® SamplePrep, Metuchen, NJ, USA). The starting powders were ABCR (ABCR GmbH & Co. KG, Karlsruhe, Germany) products: Al (99.7% purity, 325 mesh) and Fe (99.9% purity, 200 mesh). The ball-to-powder ratio was about 10:1. The total milling time was 35 h.

The produced $Al_{80}Fe_{20}$ alloy powder was blended with 20, 30, and 40 vol.% of elemental Al powder and milled for 20 min with low intensity (ball-to-powder weight ratio 3:1) to ensure uniform mixture of the two components. Low-intensity milling was carried out under argon atmosphere in a SPEX 8000 D mill.

The $Al_{80}Fe_{20}$-Al powder mixtures were consolidated using a press (ASEA, Västerås, Sweden) equipped with a toroid-type high-pressure cell (Institute for High Pressure Physics of the Russian Academy of Sciences. Troitsk, Moscow Region, Russia). The sample was placed inside a graphite tube with 1 mm thick wall serving as a resistance heater. The heater was enclosed in a toroidal container made of lithographic limestone with a 25 mm outer diameter. The assembly was compressed uniaxially between two tungsten carbide

anvils using a press. The anvils' shape and the gasket's material ensure that the pressure conditions are close to isostatic. The compaction processes were performed under a pressure of 7.7 GPa for 3 min. Pressure of 7.7 GPa was achieved with a compression force of 400 Tonnes. The pressing temperature was in the range of 600–800 °C. Pellets were loaded at the rate of 0.5 GPa/min prior to heating. The heating and cooling rate was 1000 °C/min. The consolidated samples were cylindrical in shape with a diameter of 5 mm and a height of about 4 mm.

The X-ray diffraction (XRD) investigations of the powders and consolidated samples were carried out in a Rigaku MiniFlex II X-ray diffractometer (Rigaku Corporation, Tokyo, Japan) operating with CuKα radiation.

A Hitachi S-3500N scanning electron microscope (SEM) (Hitachi high-tech corporation, Tokyo, Japan), equipped with an energy dispersive spectroscopy system (EDS), was used for examinations of the low-intensity milled powder mixtures and for the determination of chemical composition. Cross-section samples for SEM investigations were prepared by embedding the powder in a conducting resin and subsequently grinding and polishing it.

Particle size distribution measurements for the low-intensity milled powder mixtures were performed using a KμK mini3D (Kamika Instruments, Warszawa, Poland) analyser.

A Zeiss AXIOVERT 40 MAT light microscope (Carl Zeiss MicroImaging GmbH, Gottingen, Germany) and a Hitachi S-3500N SEM equipped with an EDS system were used for structural investigations and chemical analysis of the consolidated material. Bulk samples for these microscopy investigations were prepared by standard polishing techniques.

EBSD examination of a consolidated sample was performed using a Quanta 3D FEG high-resolution scanning electron microscope (FEI Company, Hillsboro, OR, USA). The sample for the EBSD investigation was prepared by grinding up to 4000 SiC paper, diamond suspension polishing and polishing with 0.1 μm SiO_2 suspension.

A Zwick Roell hardness tester (ZwickRoell GmbH & Co. KG, Ulm, Germany) was employed for the measurements of Vickers hardness (HV1) of the compacted samples (average value of at least 25 indentations).

A Zwick Roell Z250 testing machine (ZwickRoell GmbH & Co. KG, Ulm, Germany) was used for uniaxial compression tests of bulk materials. Experiments were performed under displacement control at a strain rate of 10^{-4} s^{-1}.

A Gibertini E154 (Gibertini Elettronica, Milano, Italy) balance equipped with a device for measuring the density of solids was employed for the determination of the bulk samples density (Archimedes method). The mass measurements performed allowed to calculate the open porosity of the consolidated samples.

3. Results and Discussion

Phase development and structural evolution in the $Al_{80}Fe_{20}$ powder mixture during mechanical alloying was studied by recoding of XRD patterns of the powders after various milling times (Figure 1). In the early stage of mechanical alloying (up to 15 h), a Fe(Al) solid solution was formed. This is evidenced by the gradual decrease in the intensity of the Al diffraction peaks compared to that of the Fe peaks and by the appearance of an asymmetry of the Fe diffraction profiles, which become wider on the low-angle side. Such features of the diffraction patterns accompanying the formation of a Fe(Al) solid solution were analysed in our earlier work [15]. In the diffraction pattern taken after 20 h of milling, a few broad peaks of low intensity appear. These peaks are assigned to Al_5Fe_2 intermetallic phase. In the pattern for 25 h-milled powder, more well-defined peaks of an Al_5Fe_2 phase are visible. In the XRD pattern after 30 h of milling, the peaks of Al and Fe(Al) are not present, which indicates that all the Al reacted with Fe, creating Al_5Fe_2 intermetallic, are at least partially ordered. Additionally, in the pattern of the 35 h-milled powders, only the peaks of Al_5Fe_2 phase are present. The observed phase evolution during mechanical alloying of the $Al_{80}Fe_{20}$ powder mixture is similar to that described earlier [14].

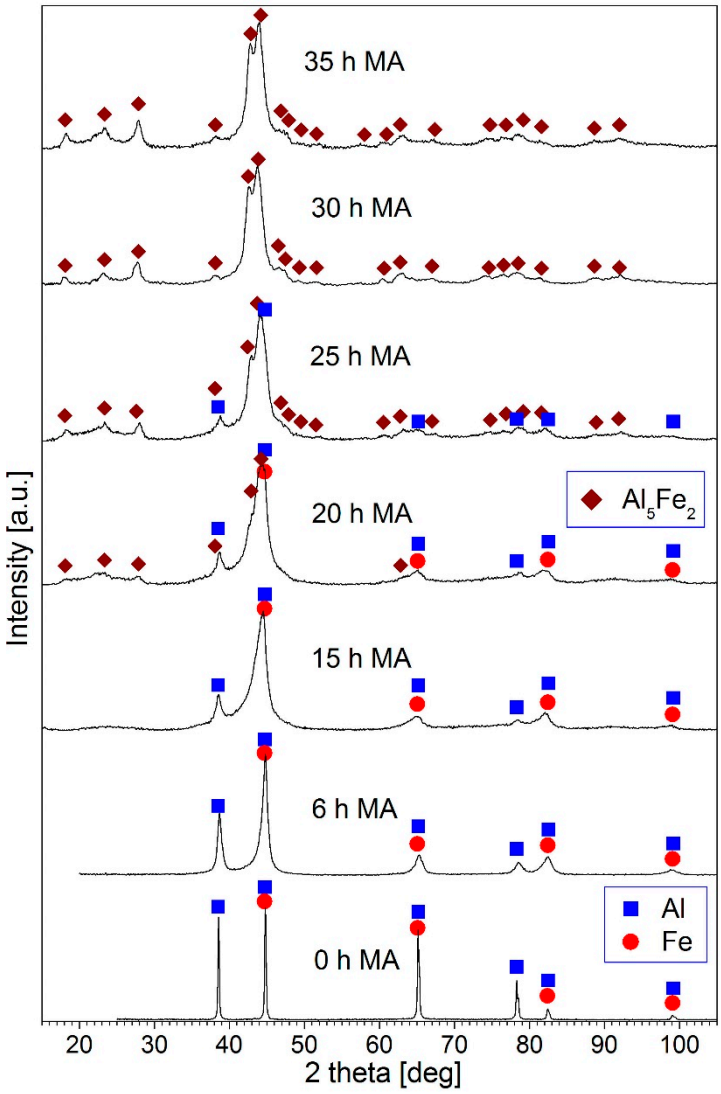

Figure 1. XRD patterns of the $Al_{80}Fe_{20}$ powder mixture milled for the times quoted.

In the Fe-Al phase equilibrium diagram, the Al_5Fe_2 phase exists for the Al concentration of 70–72 at.% [16]. Thus, the produced $Al_{80}Fe_{20}$ alloy powder has a metastable phase composition. Mechanical alloying is a nonequilibrium process and the phase composition of its products most often differs from that expected from the phase equilibrium diagrams.

It was found that, during the heating of the mechanically alloyed $Al_{80}Fe_{20}$ powder in a calorimeter up to 720 °C, the Al_5Fe_2 phase transformed into the $Al_{13}Fe_4$ [14]. For the concentration of 80% Al, there is a two-phase $Al_{13}Fe_4$+Al area in the Fe-Al phase equilibrium diagram [16]. Hence, the heating in a calorimeter moved the phase composition of the powder towards equilibrium.

There are also reports on synthesis of an unknown Al-rich phase [17] or an amorphous phase [18,19] by mechanical alloying of an $Al_{80}Fe_{20}$ powder mixture. Even for the same composition of the initial powder mixture, products of differing phase composition and structure can be synthesised by mechanical alloying, depending on applied parameters, such as type of mill, milling intensity, etc. [4,14].

In the XRD patterns of the powders after milling time longer than 6 h, all the diffraction peaks are broad, which indicates nanometric crystallite size in the phases existing in the powders.

The produced $Al_{80}Fe_{20}$ alloy powder was blended with 20, 30, or 40 vol.% of Al and subjected to short-term low-energy milling. In the XRD patterns of the processed mixtures, only the diffraction peaks of Al_5Fe_2 and Al are visible (see Figures 2a and 3a,c). Thus, the

low-energy milling processes did not cause any reactions between the phases present in the powder blends.

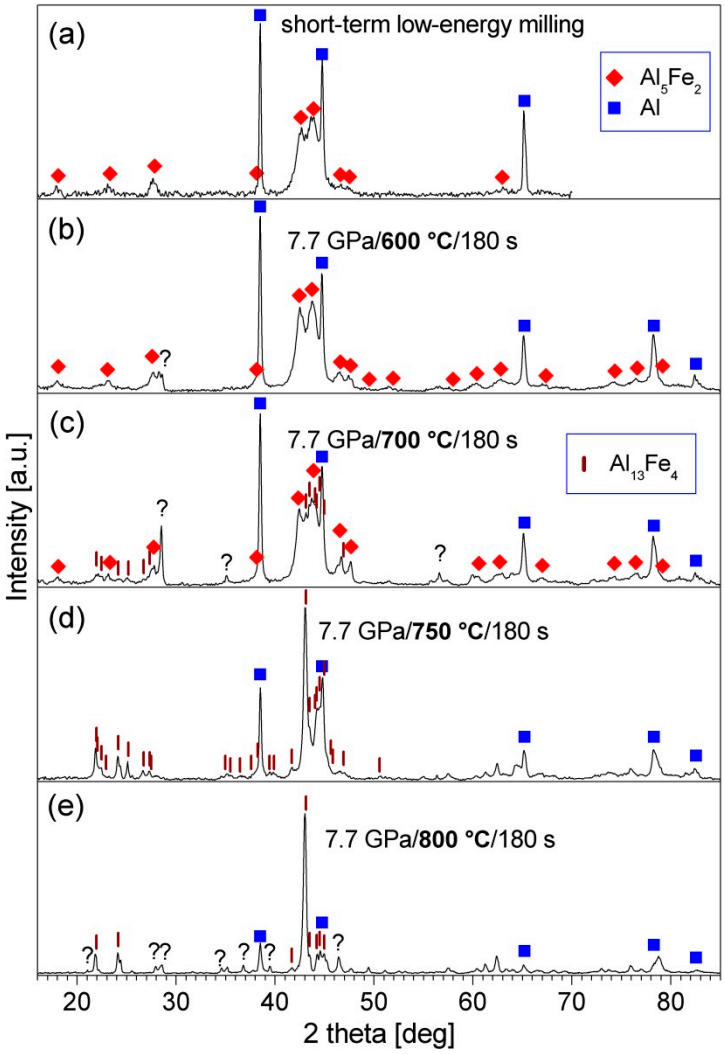

Figure 2. XRD patterns of the $Al_{80}Fe_{20}$-30%Al powder after: (**a**) short-term low-energy milling, (**b**) short-term low-energy milling and consolidation at 600 °C, (**c**) short-term low-energy milling and consolidation at 700 °C, (**d**) short-term low-energy milling and consolidation at 750 °C, and (**e**) short-term low-energy milling and consolidation at 800 °C.

To analyse particle size variation and particle shape, the powders after short-term low-energy milling were subjected to particle size distribution measurements and SEM investigations. Figure 4 illustrates particle size distribution for the short-term low-energy milled $Al_{80}Fe_{20}$-40%Al powder mixture as an example. The mean equivalent diameter of powder particles for this sample is 24.8 µm. For the other short-term low-energy milled powder mixtures, similar particle size distribution was found, and the mean equivalent diameter was 23.5 µm and 22.0 µm for the $Al_{80}Fe_{20}$-30%Al and $Al_{80}Fe_{20}$-20%Al powder mixtures, respectively.

Figure 5 shows SEM images of the loose powder of the short-term low-energy milled $Al_{80}Fe_{20}$-40%Al mixture as an example. In the powder mixture, two kinds of particles are visible: one, of almost spherical shape, visible as bright in BSE mode, and the other, with lamellar shape (Figure 5c), visible as grey in BSE mode (Figure 5b).

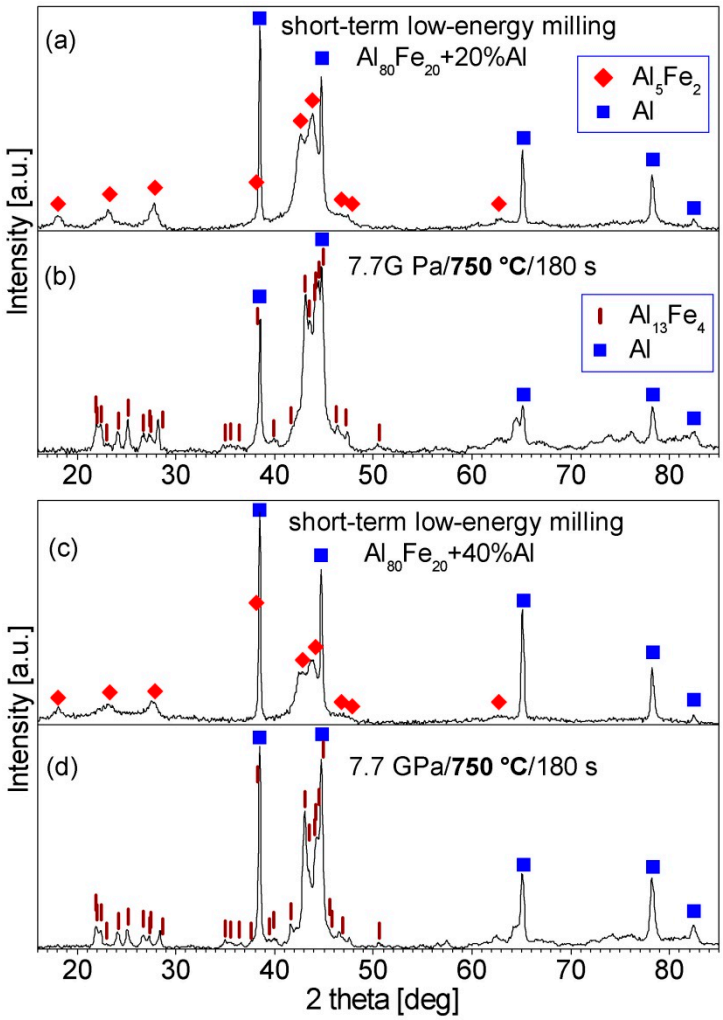

Figure 3. XRD patterns of the $Al_{80}Fe_{20}$-20%Al powder and $Al_{80}Fe_{20}$-40%Al powder after: (**a**,**c**) short-term low-energy milling, (**b**,**d**) short-term low-energy milling, and consolidation at 750 °C.

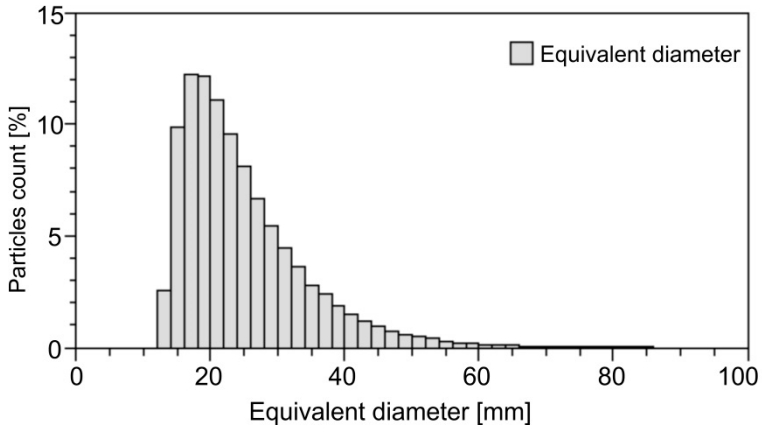

Figure 4. Particle size distribution for the short-term low-energy milled $Al_{80}Fe_{20}$-40%Al powder mixture.

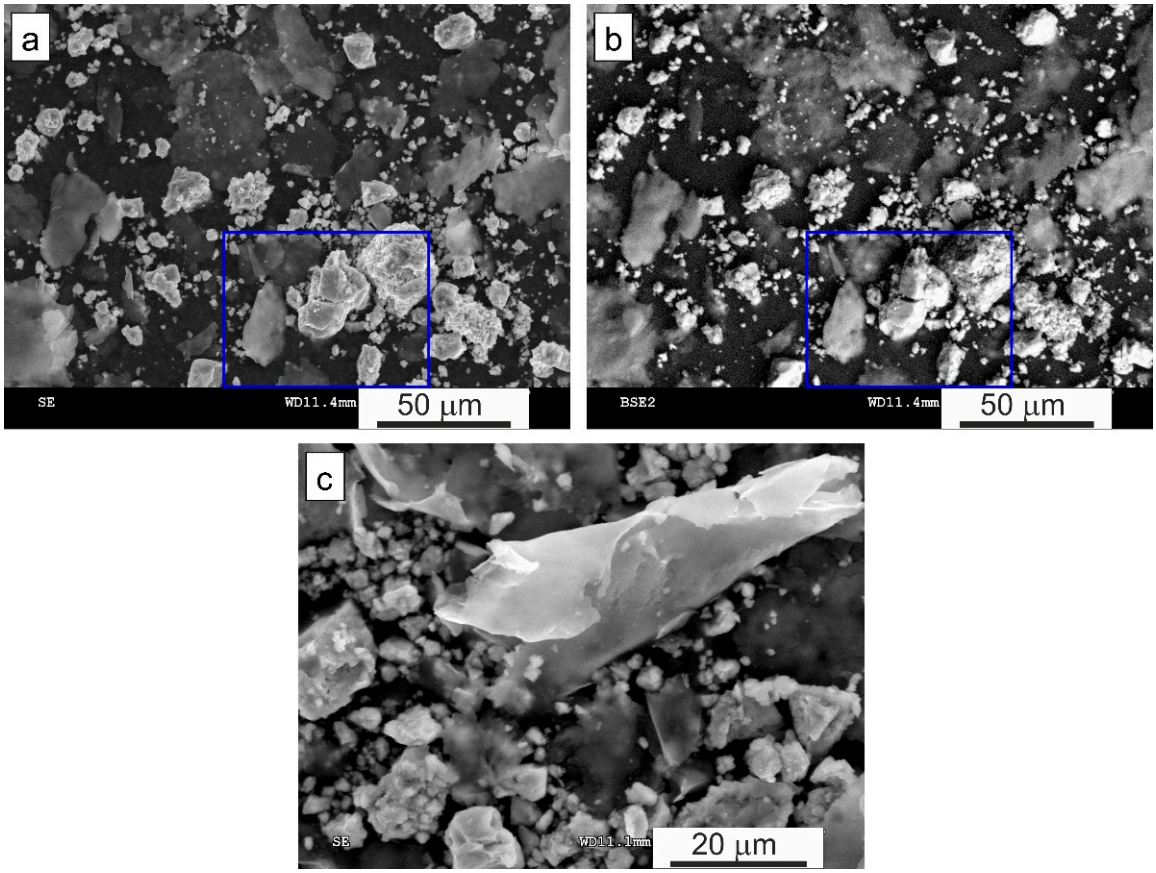

Figure 5. SEM images of the loose powder of the short-term low-energy milled $Al_{80}Fe_{20}$-40%Al mixture: (**a**) SE mode, (**b**) BSE mode (the rectangle marks the area selected for the EDS analysis, shown in Figure 6), and (**c**) SE mode (higher magnification).

EDS investigations revealed that the spherical particles are the $Al_{80}Fe_{20}$ alloy powder, while the lamellar particles are pure Al (Figure 6).

The alloy powder particles are mostly agglomerates, but there also exist some fine individual particles (Figure 5). Figure 7 depicts cross-section of an alloy powder particle. The EDS analysis of the alloy powder particles cross-sections demonstrated that the particles are chemically homogeneous, with an average composition of 78.5% Al and 21.5% Fe, as well as a composition fluctuation of 1%. For this composition, there is also a two-phase $Al_{13}Fe_4$+Al area in the Fe-Al phase equilibrium diagram [16]. Departure from the initial composition often occurs during mechanical alloying when one of the ground metals is much more plastic than the other and may stick to the grinding media (balls or container) a bit.

The prepared $Al_{80}Fe_{20}$-Al powders were consolidated by hot-pressing. The purpose was to produce a composite built of a nanocrystalline matrix, which is an $Al_{13}Fe_4$ phase (closer to the equilibrium state than an Al_5Fe_2 one for the $Al_{80}Fe_{20}$ composition) and an Al network that wraps around the matrix areas.

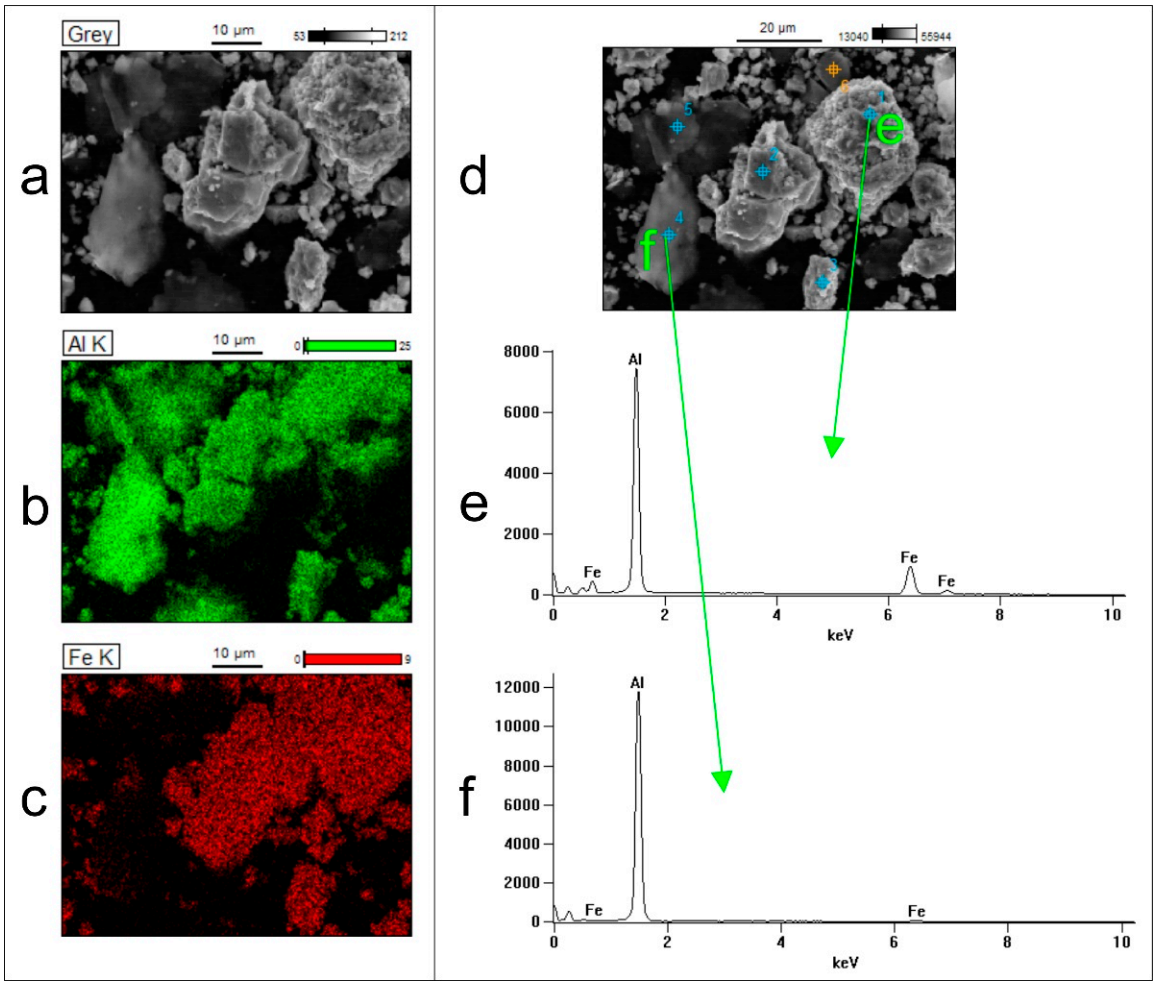

Figure 6. Results of EDS analysis of the area indicated in Figure 5: (**a**) SEM image, (**b**) EDS map with Al signal, (**c**) EDS map with Fe signal, (**d**) selected points for EDS analysis, (**e**) EDS spectrum taken in the point marked as "e" in (**d**), and (**f**) EDS spectrum taken in the point marked as "f" in (**d**).

The use of high temperature during the consolidation of powders facilitates obtaining high quality compaction. However, in the case of multiphase powders, the application of high temperature can result in a reaction between phases. We reported this in the case of two-phase powders containing Al [11,20,21]. Therefore, the appropriate temperature must be used: high but not high enough to cause uncontrolled reactions. To select the pressing temperature, the $Al_{80}Fe_{20}$-30%Al powder was consolidated at 600, 700, 750, and 800 °C. The melting point of Al under atmospheric pressure is 660.3 °C, and increases with increasing pressure up to about 1180 °C at 7.7 GPa [22]. Thus, under the pressure applied in our work, we did not expect the melting of Al during consolidation at 700, 750, and 800 °C.

The XRD patterns of the $Al_{80}Fe_{20}$-30%Al powder before and after consolidation are shown in Figure 2. XRD investigations revealed that: (i) after consolidation at 600 and 700 °C, besides Al, the Al_5Fe_2 phase is still present in the material; (ii) during consolidation at 750 °C the Al_5Fe_2 phase transformed into the $Al_{13}Fe_4$ phase; (iii) during consolidation at 800 °C $Al_{13}Fe_4$ phase and unidentified phases formed. Based on these results, the temperature of 750 °C was chosen for the hot-pressing of the two other powders. In the XRD patterns of both consolidated powders, the diffraction peaks of the $Al_{13}Fe_4$ phase and Al are present (Figure 3b,d). Overlapping of the peaks of the $Al_{13}Fe_4$ phase made it impossible to reliably estimate the crystallite size of this phase, but the width of the peaks indicates the presence of a nanocrystalline structure in this phase.

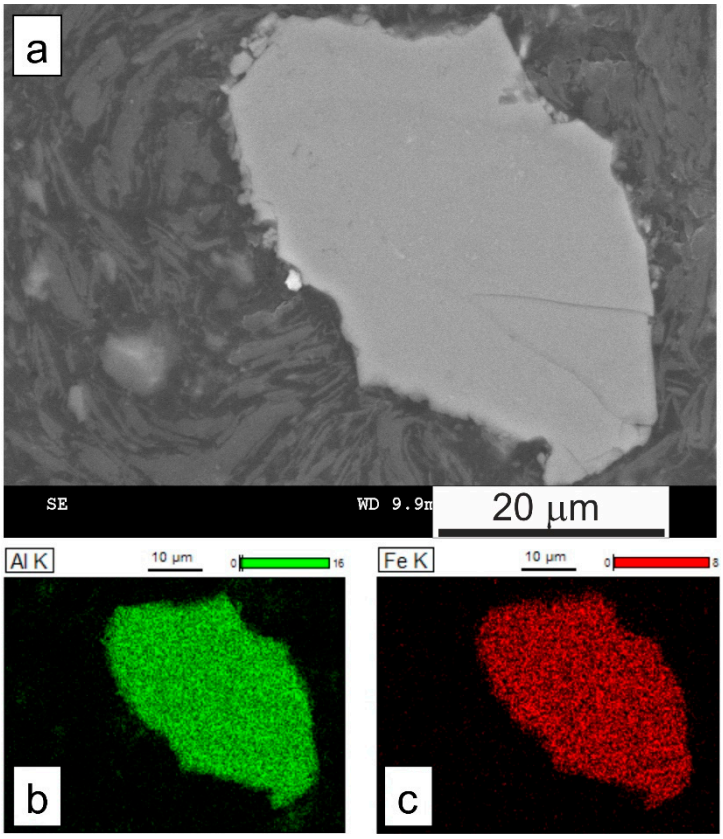

Figure 7. (**a**) SEM image of the cross-section of alloy powder particle in the short-term low-energy milled $Al_{80}Fe_{20}$-40%Al mixture: (**b**) EDS map for Al, (**c**) EDS map for Fe.

Light microscopy (LM) and SEM methods were used to observe the microstructure of the bulk samples and check the quality of consolidation. Examples of microstructure and EDS maps of the consolidated samples are shown in Figures 8 and 9, respectively. The microstructure consists of matrix areas (dark in LM, bright in SEM), wrapped around by networking regions (bright in LM, dark in SEM). LM micrographs show that the share of the wrapping networking regions is larger in the samples with higher content of Al. Examples of EDS maps of the $Al_{13}Fe_4$–20%Al sample (Figure 9) show that the matrix areas contain Al and Fe, while in the wrapping regions, only Al is present. Microscopy observation, coupled with the XRD and EDS results, indicates that the networking regions are Al and the other areas make up the $Al_{13}Fe_4$ matrix. Thus, the bulk samples have $Al_{13}Fe_4$-Al composite microstructure. Similar microstructure, i.e., Al wrapping networking regions between regions of the nanocrystalline matrix, was obtained in the case of Al_3Ni_2-Al [10], Al_5Fe_2-Al [11], and TiC-Al [13] composites produced in a similar manner as the ones in this work.

Microscopy examination of the bulk samples showed that their surface is smooth, without pores, cracks, or voids.

The results of the XRD examinations of the consolidated samples, presented above, indicated the presence of a nanocrystalline structure in the $Al_{13}Fe_4$ phase being the composites matrix. To confirm a nanocrystallinity of the $Al_{13}Fe_4$ phase, the $Al_{80}Fe_{20}$-40%Al bulk sample was investigated in SEM by the EBSD method. Figure 10 presents the EBSD map of an area of the matrix in the bulk sample. As it can be seen, the crystallite size of the $Al_{13}Fe_4$ phase is below 100 nm. Thus, the produced bulk composites have nanocrystalline matrix. The preservation of the nanocrystalline structure of the intermetallic phase, during consolidation at high temperatures, is due to the use of high pressing pressure, as we have shown previously [7,8]. Since diffusion is involved in grain growth, the influence of pressure apparently comes from the fact that the diffusion coefficient decreases with the

increase in pressure, usually by a factor ranging from 2 to 10 for a pressure of 1 GPa [23]. Hence, the use of high pressure during consolidation can reduce the mobility of grain boundaries at high temperature.

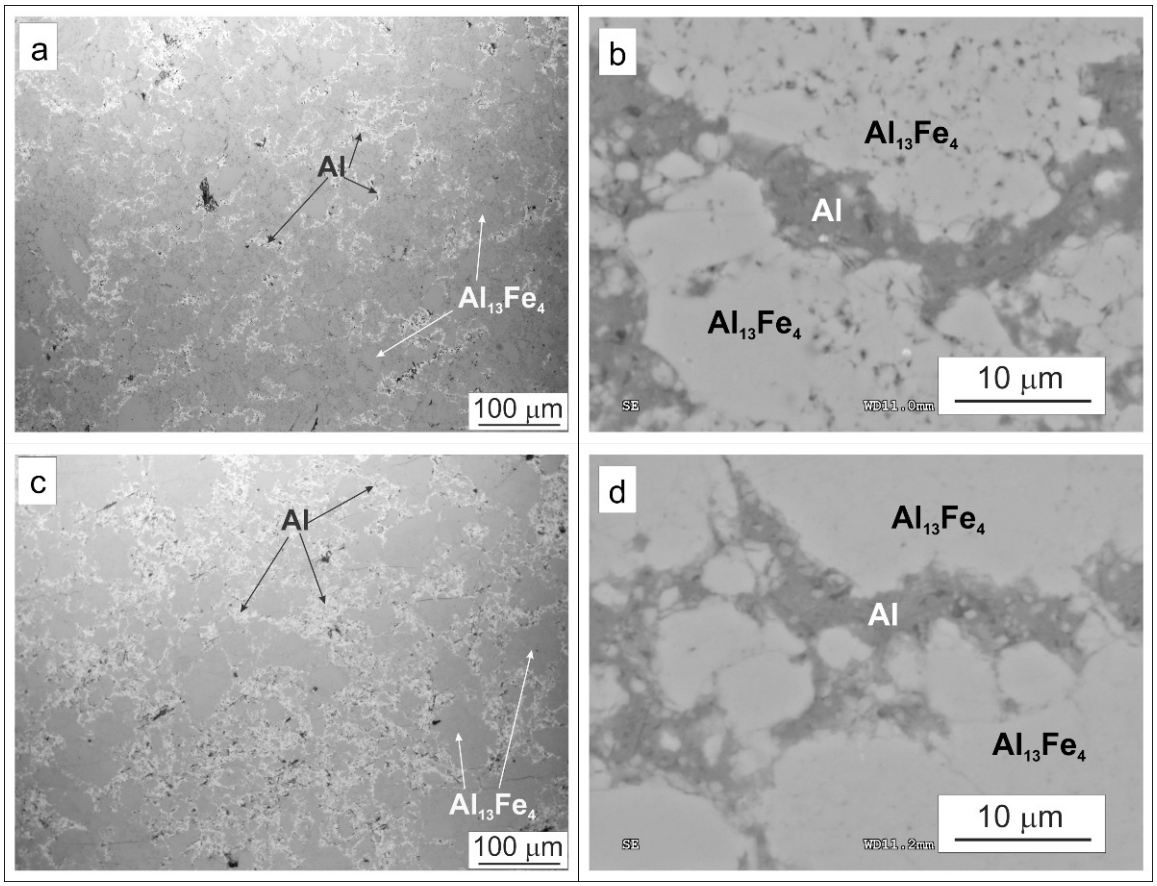

Figure 8. Micrographs of the $Al_{80}Fe_{20}$-20%Al bulk composite: (**a**) LM, (**b**) SEM, and micrographs of the $Al_{80}Fe_{20}$-40%Al composite: (**c**) LM, (**d**) SEM.

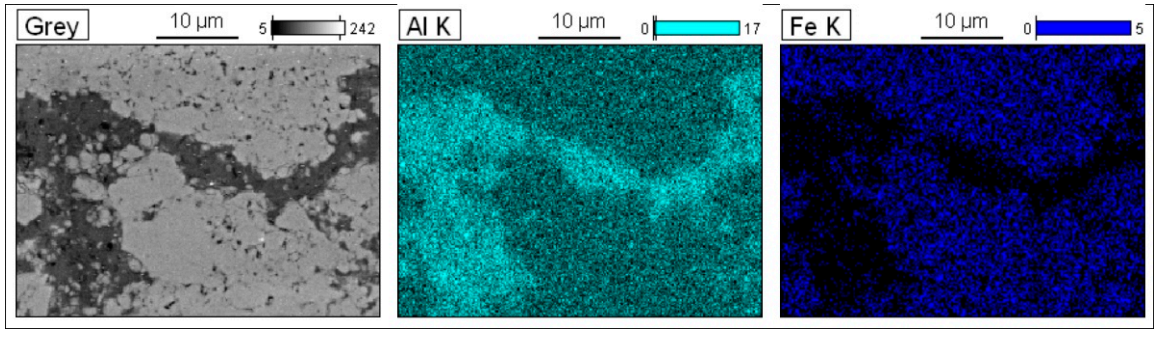

Figure 9. EDS maps of the $Al_{80}Fe_{20}$-20%Al bulk composite.

The produced composites were also characterised by compression tests, as well as hardness, density, and open porosity measurements. The hardness, compressive strength, plastic strain, and density values are given in Table 1.

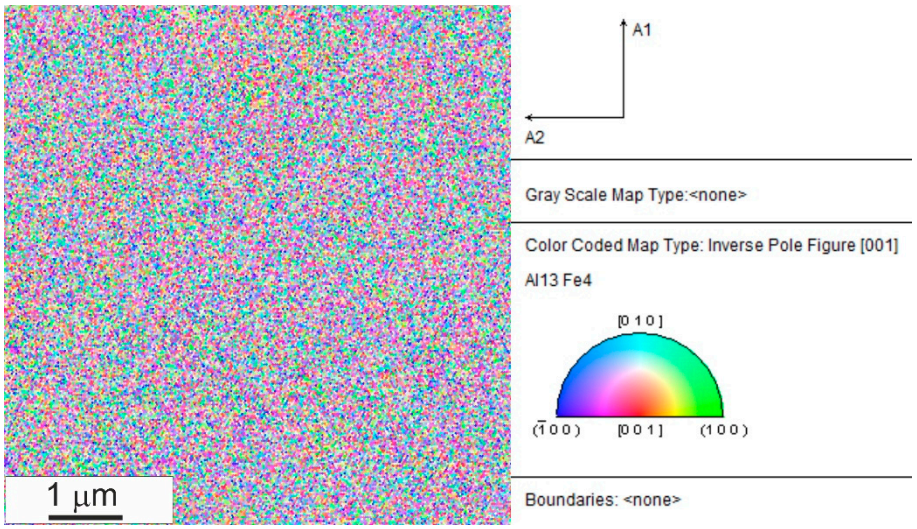

Figure 10. The EBSD inverse pole figure map of the matrix in the $Al_{80}Fe_{20}$-40%Al bulk sample.

Table 1. Values of hardness (HV1), ultimate compressive stress (σ_{UCS}), plastic strain (ε_p), and density (ρ) of the produced composites.

Material	HV1 [GPa]	σ_{UCS} [MPa]	ε_p [%]	ρ [g/cm^3]
$Al_{13}Fe_4$-20%Al	5.50	538	-	3.48
$Al_{13}Fe_4$-30%Al	5.09	805	1.5	3.42
$Al_{13}Fe_4$-40%Al	4.52	812	9.1	3.27

The hardness of the composites decreases with the increase in the networking Al regions content. However, the compressive strength of the $Al_{13}Fe_4$-30%Al and $Al_{13}Fe_4$-40%Al composites is considerably higher than that of the $Al_{13}Fe_4$-20%Al one. This is because, during the compression test, the $Al_{13}Fe_4$-20%Al sample fractured catastrophically in the elastic region, crumbling into fine pieces. This is probably due to the insufficient bonding of the powder particles during the consolidation process. The $Al_{13}Fe_4$-30%Al and $Al_{13}Fe_4$-40%Al composites, in contrast, showed some plasticity, and, after failure, remained whole. However, the composite with 30% of Al, unlike that with 40% of Al, fractured shortly after yield. Thus, the presence of more than 20% of the networking Al in the $Al_{13}Fe_4$-Al composites improved the interparticle bonding and the ductility of the material. In addition, micrometric Al grains participate in the plastic deformation, and they can also help to release stress concentrations and, thus, retard crack initiation and propagation [12]. The compressive stress–strain curves are shown in Figure 11.

For the in-situ Al-$Al_{13}Fe_4$ composite, prepared by mechanical alloying of $Al_{90}Fe_{10}$ powder mixture followed by spark plasma sintering, the microhardness HV0.3 of 1.97 GPa and the compressive strength of 1130.1 MPa (but without any plasticity of material) were reported [24]. No other information concerning $Al_{13}Fe_4$-Al composites was found in the literature.

The density of the produced composites decreases with the increase in the Al content. The open porosity in all the produced composites does not exceed 0.15%. The specific compressive strength of the composites with 40% and 30% of Al is 248 kNm/kg and 235 kNm/kg, respectively, and is higher than that of Al_5Fe_2-Al (185-190 kNm/kg [11]) and Al3Ni2-Al (146-207 kNm/kg [10]) composites.

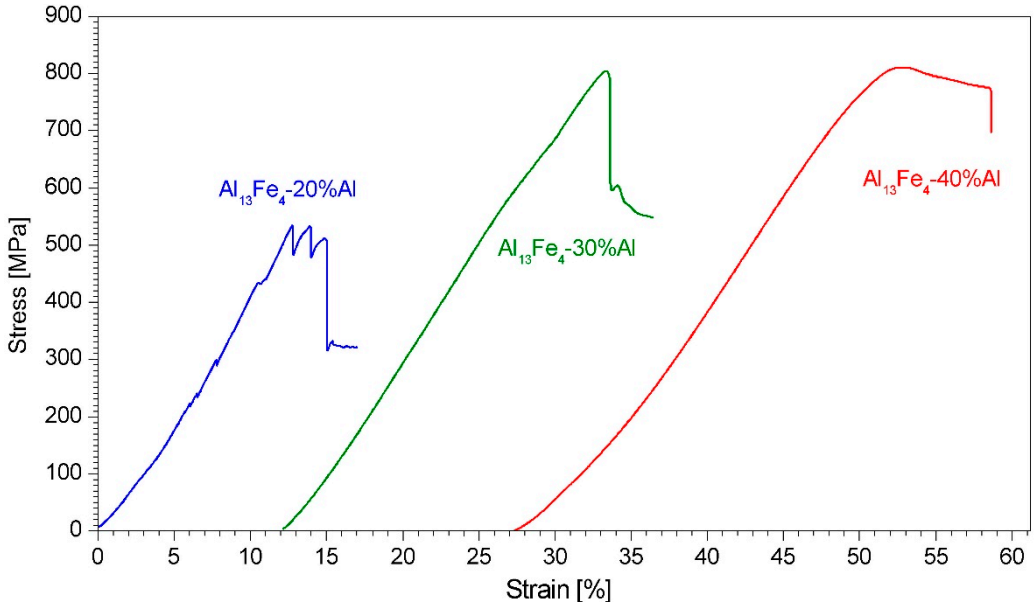

Figure 11. Compressive stress–strain curves of the consolidated Al-$Al_{13}Fe_4$ composites. The curves are shifted relative to each other for clarity.

4. Conclusions

Mechanically alloyed $Al_{80}Fe_{20}$ powder containing a metastable nanocrystalline Al_5Fe_2 phase was used as a matrix for the composites. $Al_{80}Fe_{20}$-X vol.% Al (X = 20, 30, and 40) powder mixtures were consolidated by hot-pressing. Hot-pressing tests have shown that the temperature of 750 °C is suitable for the consolidation, during which only the transformation of the Al_5Fe_2 phase into the nanocrystalline $Al_{13}Fe_4$ phase occurs, without other reactions. The microstructure of the bulk samples consisted of $Al_{13}Fe_4$ intermetallic matrix areas wrapped around by networking Al regions. With the increase in Al content, the hardness of the composites decreased, ranging from 4.52 to 5.50 GPa. The $Al_{13}Fe_4$-20%Al composite failed in the elastic region, while the composites with 30% and 40% of Al showed some plasticity: namely, 1.5% and 9.1%, respectively. The presence of more than 20% of Al in the $Al_{13}Fe_4$-Al composites improved their ductility. The compressive strength of the composites containing 30 and 40% of Al was 805 and 812 MPa, respectively, and it was considerably higher than that of the $Al_{13}Fe_4$-20%Al composite (538 MPa). The low-density materials produced have a relatively high hardness.

Author Contributions: Conceptualization, M.K.; methodology, M.K.; validation, M.K.; formal analysis, M.K.; investigation, M.K., S.G. and D.Z.; resources, M.K., S.G. and D.Z.; writing—original draft preparation, M.K.; writing—review and editing, M.K., S.G. and D.Z.; visualization, M.K. and D.Z.; supervision, M.K.; project administration, M.K.; funding acquisition, M.K. and D.Z. All authors have read and agreed to the published version of the manuscript.

Funding: This research was funded by the National Science Centre, Poland, grant number N N507 217440. The financial support from the subsidy of Faculty of Materials Science and Engineering, Warsaw University of Technology is gratefully acknowledged. The authors would like to thank for the funding from the statutory sources of the Military University of Technology (project No. 22-790/2022/WAT).

Institutional Review Board Statement: Not applicable.

Informed Consent Statement: Not applicable.

Data Availability Statement: Data sharing not applicable.

Conflicts of Interest: The authors declare no conflict of interest.

References

1. Kratochvil, P.; Šima, V. Preface. *Intermetallics* **2010**, *18*, 1263–1264. [CrossRef]
2. Hahn, E.N.; Meyers, M.A. Grain-size dependent mechanical behavior of nanocrystalline metals. *Mater. Sci. Eng. A* **2015**, *646*, 101–134. [CrossRef]
3. Li, J.C.M. *Mechanical Properties of Nanocrystalline Materials*; Pan Stanford Publishing: Singapore, 2011.
4. Suryanarayana, C. Mechanical alloying and milling. *Progr. Mat. Sci.* **2001**, *46*, 1–184. [CrossRef]
5. Koch, C.C.; Ovid'ko, I.A.; Seal, S.; Veprek, S. *Structural Nanocrystalline Materials: Fundamentals and Applicatios*; Cambridge University Press: Cambridge, UK, 2007.
6. Koch, C.C. Optimization of strength and ductility in nanocrystalline and ultrafine grained metals. *Scr. Mater.* **2003**, *49*, 657–662. [CrossRef]
7. Krasnowski, M.; Kulik, T. Nanocrystalline FeAl matrix composites reinforced with TiC obtained by hot-pressing consolidation of mechanically alloyed powders. *Intermetallics* **2007**, *15*, 1377–1383. [CrossRef]
8. Krasnowski, M.; Gierlotka, S.; Kulik, T. FeAl-B composites with nanocrystalline matrix produced by consolidation of mechanically alloyed powders. *J. Alloys Compd.* **2019**, *791*, 75–80. [CrossRef]
9. Witkin, D.; Lee, Z.; Rodriquez, R.; Nutt, S.; Lavernia, E.J. Al–Mg alloy engineered with bimodal grain size for high strength and increased ductility. *Scr. Mater.* **2003**, *49*, 297–302. [CrossRef]
10. Krasnowski, M.; Gierlotka, S.; Kulik, T. Al_3Ni_2–Al composites with nanocrystalline intermetallic matrix produced by consolidation of milled powders. *Adv. Powder Technol.* **2014**, *23*, 1362–1368. [CrossRef]
11. Krasnowski, M.; Gierlotka, S.; Kulik, T. Nanocrystalline Al_5Fe_2 intermetallic and Al_5Fe_2–Al composites manufactured by high-pressure consolidation of milled powders. *J. Alloys Compd.* **2016**, *656*, 82–87. [CrossRef]
12. Fan, G.J.; Choo, H.; Liaw, P.K.; Lavernia, E.J. Plastic deformation and fracture of ultrafine-grained Al–Mg alloys with a bimodal grain size distribution. *Acta Mater.* **2006**, *54*, 1759–1766. [CrossRef]
13. Krasnowski, M.; Gierlotka, S.; Kulik, T. TiC–Al composites with nanocrystalline matrix produced by consolidation of milled powders. *Adv. Powder Technol.* **2015**, *26*, 1269–1272. [CrossRef]
14. Krasnowski, M.; Kulik, T. Nanocrystalline and amorphous Al–Fe alloys containing 60–85% of Al synthesised by mechanical alloying and phase transformations induced by heating of milling products. *Mater. Chem. Phys.* **2009**, *116*, 631–637. [CrossRef]
15. Krasnowski, M.; Grabias, A.; Kulik, T. Phase transformations during mechanical alloying of Fe-50% Al and subsequent heating of the milling product. *J. Alloys Compd.* **2006**, *424*, 119–127. [CrossRef]
16. Li, X.; Scherf, A.; Heilmaier, M.; Stein, F. The Al-rich part of the Fe-Al diagram. *J. Phase Equilibria Diffus.* **2016**, *37*, 162–173. [CrossRef]
17. Cardellini, F.; Contini, V.; Gupta, R.; Mazzone, G.; Montone, A.; Perin, A.; Principi, G. Microstructural evolution of Al–Fe powder mixtures during high-energy ball milling. *J. Mater. Sci.* **1998**, *33*, 2519–2527. [CrossRef]
18. Huang, B.; Ishihara, K.N.; Shingu, P.H. Metastable phase of Al–Fe system by mechanical alloying. *Mater. Sci. Eng. A* **1997**, *231*, 72–79. [CrossRef]
19. Zhou, F.; Lück, R.; Scheffer, M.; Lang, D.; Lu, K. The crystallization process of amorphous $Al_{80}Fe_{20}$ alloy powders prepared by ball milling. *J. Non-Cryst. Solids* **1999**, *250–252*, 704–708. [CrossRef]
20. Krasnowski, M.; Gierlotka, S.; Kulik, T. Nanocrystalline matrix Al_3Ni_2–Al–Al_3Ni composites produced by reactive hot-pressing of milled powders. *Intermetallics* **2014**, *54*, 193–198. [CrossRef]
21. Krasnowski, M.; Gierlotka, S.; Kulik, T. Nanocrystalline matrix TiC–Al_3Ti and TiC–Al_3Ti–Al composites produced by reactive hot-pressing of milled powders. *Adv. Powder Technol.* **2014**, *25*, 1082–1086. [CrossRef]
22. Errandonea, D. The melting curve of ten metals up to 12 GPa and 1600 K. *J. Appl. Phys.* **2010**, *108*, 033517. [CrossRef]
23. Mehrer, H. Diffusion: Introduction and Case Studies in Metals and Binary Alloys. In *Diffusion in Condensed Matter*; Heitjans, P., Karger, J., Eds.; Springer: Berlin/Heidelberg, Germany, 2005; pp. 3–63.
24. Gu, J.; Gu, S.; Xue, L.; Wu, S.; Yan, Y. Microstructure and mechanical properties of in-situ $Al_{13}Fe_4$/Al composites prepared by mechanical alloying and spark plasma sintering. *Mater. Sci. Eng. A* **2012**, *558*, 684–691. [CrossRef]